



Published in final edited form as:

J Mol Biol. 2011 July 15; 410(3): 447–460. doi:10.1016/j.jmb.2011.05.016.

Characterization of the Structure and Function of *Klebsiella pneumoniae* Allantoin Racemase

Jarrod B. French¹, David B. Neau^{1,2}, and Steven E. Ealick^{1,*}

¹Department of Chemistry and Chemical Biology, Cornell University, Ithaca, New York 14853, USA

²NE-CAT, Argonne National Laboratory, Argonne, Illinois, 60439, USA

Abstract

The oxidative catabolism of uric acid produces 5-hydroxyisourate (HIU), which is further degraded to (*S*)-allantoin by two enzymes, HIU hydrolase and 2-oxo-4-hydroxy-4-carboxy-5-ureidoimidazole (OHCU) decarboxylase. The intermediates of the latter two reactions, HIU and OHCU, are unstable in solution and decay nonstereospecifically to allantoin. In addition, non-enzymatic racemization of allantoin has been shown to occur at physiological pH. Since the further breakdown of allantoin is catalyzed by allantoinase, an enzyme that is specific for (*S*)-allantoin, an allantoin racemase is necessary for complete and efficient catabolism of uric acid. In this work we characterize the structure and activity of allantoin racemase from *Klebsiella pneumoniae* (KpHpxA). In addition to an unliganded structure solved using SeMet-SAD, structures of C79S/C184S-KpHpxA in complex with allantoin and with 5-acetylhydantoin are presented. These structures reveal several important features of the active site including an oxyanion hole and a polar binding pocket that interacts with the ureido tail of allantoin and serves to control the orientation of the hydantoin ring. The ability of KpHpxA to interconvert the (*R*)- and (*S*)- enantiomers of allantoin is demonstrated and analysis of the steady state kinetics of KpHpxA yielded a k_{cat}/K_M of $6.0 \times 10^5 \text{ M}^{-1}\text{s}^{-1}$. Mutation of either of the active site cysteines, Cys79 or Cys184, to serine, inactivates this enzyme. The data presented provides new insights into the activity and substrate specificity of this enzyme and enables us to propose a mechanism for catalysis that is consistent with the two-base mechanism observed in other members of the Aspartate/Glutamate family.

Keywords

purine catabolism; ureide; X-ray crystallography; racemization; hydantoin

© 2011 Elsevier Ltd. All rights reserved

*Corresponding author: Steven Ealick, 120 Baker Lab, Cornell University, Ithaca, NY 14853-1301, USA; Phone: (607) 255-7961; Fax: (607) 255-1227; see3@cornell.edu.

Publisher's Disclaimer: This is a PDF file of an unedited manuscript that has been accepted for publication. As a service to our customers we are providing this early version of the manuscript. The manuscript will undergo copyediting, typesetting, and review of the resulting proof before it is published in its final citable form. Please note that during the production process errors may be discovered which could affect the content, and all legal disclaimers that apply to the journal pertain.

Accession numbers The atomic coordinates and structure factors for KpHpxA have been deposited in the Protein Data Bank with accession numbers 3QVJ, 3QVK, and 3QVL for the unliganded KpHpxA, KpHpxA-allantoin complex and KpHpxA-5-acetylhydantoin complex structures, respectively.

Introduction

The enzymatic degradation of uric acid is the final stage of purine catabolism and serves in plants and some bacteria to provide a source of nitrogen, particularly when other nitrogen sources are depleted (Scheme 1).^{1,2} The first stage of this pathway involves three enzymes and facilitates the stereospecific oxidative decomposition of uric acid to (*S*)-allantoin. Upon oxidation by urate oxidase, two additional enzymes, 5-hydroxyisourate (HIU) hydrolase and 2-oxo-4-hydroxy-4-carboxy-5-ureidoimidazoline (OHCU) decarboxylase, complete the conversion from urate to (*S*)-allantoin.^{3–5} While the product of these enzymatic conversions is solely the (*S*)- enantiomer, non-enzymatic decomposition of both HIU and OHCU can occur and does so nonstereospecifically. In addition, slow, non-enzymatic racemization of allantoin has been observed to occur.⁶

The conversion of allantoin to allantoate by an allantoinase enzyme is a point of convergence in the metabolism of ureides.^{1,2,7} This step is present in all organisms that catabolize allantoin. To date two types of allantoinase have been identified, a metal-dependent form and a metal-independent form.^{8–10} While these two enzymes may differ in mechanism, they both preferentially bind the (*S*)- enantiomer of allantoin. Considering the selectivity of the allantoinase enzymes and the various mechanisms operating to produce racemic mixtures of allantoin, efficient use of this molecule would require the presence of a racemase enzyme. Recent genetic studies on *Klebsiella sp.* have identified a gene cluster for purine utilization that encodes several enzymes that catalyze novel chemical transformations, including an enzyme that was putatively identified as an allantoin racemase.^{11,12} This enzyme shares 45% identity over 96% of its length with the hydantoin racemase from *Pseudomonas sp.*

While enzymatic racemization of allantoin was noted as early as the 1970's,^{13–15} there has been very little reported in the subsequent three decades. Despite this paucity of data on allantoin racemase, some progress has been made on the characterization of the homologous hydantoin racemase.¹⁶ This enzyme belongs to the Aspartate/Glutamate racemase superfamily and is known to catalyze racemization of 5-substituted hydantoin in a cofactor- and metal-independent fashion. Hydantoin racemase, which catalyzes the racemization of various 5-substituted hydantoin, is a commercially important biocatalyst used in the production of optically pure amino acids.¹⁷

Hydantoin racemase and other members of the Aspartate/Glutamate racemase superfamily are believed to operate using a two-base mechanism that involves a pair of highly conserved cysteine residues.^{18,19} Binding and kinetic studies combined with site-directed mutagenesis have demonstrated the importance of these two cysteines for both substrate recognition and catalysis. While this enzyme can bind and catalyze the conversion of both isomers, it has been reported that it does so with differing specificity. Much of the binding and catalytic selectivity for the different isomers has been attributed to the two active site cysteine residues.^{19,20}

In this work we present the first X-ray crystal structures of allantoin racemase in both unliganded and ligand-bound forms. These structures from the opportunistic human pathogen *Klebsiella pneumoniae* provide valuable insights into substrate binding and selectivity. In addition, the KpHpxA catalyzed conversion of either (*R*)- or (*S*)-allantoin to the racemic mixture is demonstrated using circular dichroism (CD) spectroscopy and the steady-state kinetic parameters are reported. Mutation of either of the active site cysteine residues to serine completely abolishes the ability of the enzyme to catalyze the racemization of allantoin. Examination of the structural and biochemical data provided

herein suggests that this enzyme utilizes a conserved two-base mechanism to catalyze the racemization of allantoin.

Results

Structure of unliganded KpHpxA

The structure of KpHpxA was determined to 2.1 Å resolution using selenomethionyl (SeMet) single-wavelength anomalous dispersion (SAD) phasing. Other than the polyhistidine tag and the two N-terminal residues, the entire protein was modeled. KpHpxA is an α/β protein with two domains that form a V shape in the protomer (Fig. 1a). The two domains share a high degree of similarity (RMSD 3.1 Å), and each contains a four-stranded parallel β -sheet sandwiched between two pairs of α -helices (Figs. 1a,c). When crystallographic symmetry related molecules were considered, the crystallographic data suggested that KpHpxA formed a stable hexamer in the crystal (Fig. 1b). The quaternary structure was verified by size exclusion chromatography (data not shown). The hexamer is made up of a trimer of dimers, with the three identical dimer interfaces occurring at the groove between domains. This interface has an approximate buried surface area of 3,400 Å² and is dominated by polar contacts between amphipathic helices 4 and 9 of the two protomers. The interface between the dimers is predominantly along helices 2 and 3 and has only slightly less buried surface area (approximately 3,340 Å²) than the dimer interface itself. In addition, the C-terminal 20 residues form a loop that packs along the length of helix 2 of the neighboring molecule providing additional polar contacts. Overall, this leads to a tightly packed hexamer with a total buried surface area of approximately 22,000 Å².

The active site of KpHpxA, positively identified by the presence of allantoin or 5-acetylhydantoin in KpHpxA-ligand complexes (see below), is occupied predominantly by water molecules in the absence of ligand. In addition, a spherical region of strong electron density was observed between the backbone amides of Phe80 and Gly185, putatively identified as the oxyanion hole (see below). This density was modeled as a chloride ion in the unliganded structure of KpHpxA.

C79S/C184S KpHpxA - allantoin complex structure

In order to examine active site interactions in KpHpxA, we constructed the C79S/C184S double mutant and determined the structure in complex with allantoin. The observed difference density in the active site allowed for the unambiguous placement of the ligand (Figs. 2a, 3a). While the solution used for soaking the crystals was a mixture of the (*R*)- and (*S*)- isomers, the observed density best fit the enol form of allantoin (Fig. 2b). Most of the interactions between the enzyme and the ligand are made through the backbone of KpHpxA. A notable exception to this is a region surrounding the amide tail of the ligand where several hydrogen bonds are made to the sidechains of Thr118, Thr119, the backbone of Gly183 and to a water molecule positioned by Thr123.

The hydantoin ring of allantoin is positioned in the active site through three sets of interactions. In addition to the above-mentioned binding pocket that tightly holds the allantoin tail in place, additional interactions are made through the two oxygen atoms of the hydantoin ring. These are each held in place by a pair of residues: the backbone amide nitrogens of Phe80 and Gly185 for the C4 oxygen atom, and the backbone amide nitrogen of Ile47 and the sidechain of Asn12 for the C2 oxygen atom (Fig. 2b). Both of these pairs of hydrogen bonding interactions could also provide the necessary stabilizing interactions required for an oxyanion hole. Considering the geometry of the ligand in the active site, however, it is likely that only the former pair of residues would function in this capacity during catalysis.

The two conserved cysteine residues, Cys79 and Cys184, which are replaced by serine residues in the mutant structure, are situated on opposite sides of allantoin in the asymmetric active site of KpHpxA (Fig. 3a). In the structure of the C79S/C184S KpHpxA double mutant with allantoin bound, the electron density for the Ser79 sidechain was diffuse and was best fit by two rotamers, each having 50% occupancy (Fig. 3a). The distances between the two serine residues and C5 of allantoin in the structure are 3.2 Å for Ser79 (rotamer closest to allantoin) and 4.2 Å for Ser184. Also present in the active site is a water molecule located near Ser79 (Fig. 3a). This water molecule is 2.6 Å from Ser79 and 4.3 Å from C5 of allantoin. The water molecule also makes hydrogen bonds with the backbone nitrogen of Gly81 and the sidechain of Glu53.

Structural similarity to other proteins

A search for structurally homologous proteins using the DALI²¹ server yielded several related structures (Supplementary Table S1). As expected, all of these structures belonged to the Aspartate/Glutamate racemase superfamily of proteins. The protein of known structure that is most similar to KpHpxA is the hydantoin racemase from *Pyrococcus horikoshii* (PDB identifier 2EQ5; unpublished). The asymmetric unit contains a dimer and higher oligomerization is not allowed in the hexagonal space group $P6_5$. The orientation of the two protomers in the dimeric 2EQ5 structure is similar to that of a dimer from the KpHpxA hexamer. Primarily smaller, hydrophobic residues populate the 2EQ5 interface resulting in slightly smaller separation between the protomers compared to KpHpxA. A structural superposition of KpHpxA and 2EQ5 shows that the two proteins contain very similar secondary structure elements although some of the helical regions do not align well (Fig. 4a). In spite of the overall similarity of the two proteins, the active sites display some distinct differences (Fig. 4b).

Superposition of the active site residues of KpHpxA and 2EQ5 shows expected similarities in the conserved cysteine residues and in the putative oxyanion hole. Beyond these features, little similarity exists. Not surprisingly, the tail-binding region of the KpHpxA active site, which is populated by several threonine residues, is not present in the hydantoin racemase structure. In 2EQ5, this region is composed of predominantly non-polar residues, presumably to accommodate the typically aliphatic chains present in the 5-substituted hydantoin substrates. Additional interactions observed between allantoin and KpHpxA, particularly at the C2 oxygen atom, are not present in 2EQ5. Overall, the active site of the hydantoin racemase is larger and more open than that observed in the allantoin racemase structure of KpHpxA.

C79S/C184S KpHpxA - 5-acetylhydantoin complex structure

To further probe the active site of KpHpxA and examine how the residues contained within it determine specificity, we determined the structure of KpHpxA in complex with the allantoin analogue, 5-acetylhydantoin. Unlike allantoin, which is observed as an enol in the active site, the (*R*)- enantiomer (equivalent to the (*S*)- enantiomer of allantoin) is clearly bound to KpHpxA in this structure (Fig. 3b). While the orientation of the hydantoin ring is similar for the two ligands, the tail region makes distinctly different binding interactions. The substitution of a carbon for N6 of allantoin leads to a different geometry and moves the acetyl group away from the threonine-rich pocket of the active site. This causes a slight shift in the ring and leads to additional hydrogen bonding between the acetyl group of 5-acetylhydantoin and Ser184 of the enzyme. A similar feature in both the KpHpxA-allantoin and KpHpxA-5-acetylhydantoin structures is the electron density for the Ser79 sidechain, which is consistent with the presence of two rotamers, each having approximately 50% occupancy.

Racemization of (*R*)- and (*S*)-allantoin by KpHpxA

To demonstrate that KpHpxA functions as an allantoin racemase, we tested the ability of this enzyme to catalyze the conversion of each of the isolated enantiomers to the racemic mixture. The difference in CD spectra of the two enantiomers allowed for the facile measurement of this reaction. As shown in Fig. 5, KpHpxA catalyzes the racemization of allantoin. The rate of racemization of (*S*)- and (*R*)-isomers occurs at $183 \pm 17 \text{ s}^{-1}$ and $238 \pm 19 \text{ s}^{-1}$, respectively, six orders of magnitude faster than the non-enzymatic racemization reaction ($2 \times 10^{-4} \text{ s}^{-1}$, Supplementary Fig. S1). A fit of initial rates of reaction to the Michaelis-Menten equation yielded K_M values of $0.3 \pm 0.1 \text{ mM}$ and $0.4 \pm 0.1 \text{ mM}$ for the (*S*)- and (*R*)-isomers, respectively. The average k_{cat}/K_M for the KpHpxA catalyzed reaction is $6.0 \times 10^5 \text{ M}^{-1}\text{s}^{-1}$.

The C79S, C184S and double mutant C79S/C184S-KpHpxA were also tested for their ability to catalyze the racemization of allantoin. None of the mutant enzymes tested increased the rate of racemization over the non-enzymatic rate for either (*S*)- or (*R*)-allantoin (data not shown).

Docking of (*R*)- and (*S*)- isomers of allantoin into the KpHpxA active site

To better understand the possible substrate interactions with KpHpxA, both (*R*)- and (*S*)-allantoin were modeled into the active site of this enzyme. After positioning each isomer by superposition with the enol form of allantoin observed in the C79S/C184S KpHpxA structure, the ligand was energy-minimized while fixing the protein side chains. An overlay of the results with the structure of the double mutant KpHpxA structure with allantoin bound is shown in Fig. 6.

Discussion

Overall structure of KpHpxA

KpHpxA is a two domain, α/β protein that is structurally homologous to members of the Glu/Asp racemase superfamily. The two domains of this enzyme share the same secondary structural elements suggesting that a gene duplication and fusion event occurred at some point in this protein's evolutionary history (Figs. 1a,c). A clear hexameric quaternary structure was observed in the crystal structures of this enzyme and was confirmed by size exclusion chromatography (data not shown). The most structurally similar enzyme, hydantoin racemase from the archaeon *Pyrococcus horikoshi* (PDB 2EQ5), was observed as a dimer in the crystal structure. While all of the necessary active site contacts to the ligands are made by a single protomer in KpHpxA, a very tight dimer, similar to what is observed in the hydantoin racemase structure, is formed between neighboring protomers in the hexameric molecule (Fig. 1b). Size exclusion chromatography on hydantoin racemases from other organisms is consistent with either a hexamer²² or a tetramer.^{23,24} It is possible that the hexamer observed in the *K. pneumoniae* structure provides some evolutionary advantage in stability or activity over the dimeric form observed in the archaeal hydantoin racemase, although further characterization of the archaeal enzyme would be required to complete this analysis.

Comparison of KpHpxA to other structures

A DALI search for structural homologues of KpHpxA yielded several proteins of the Glu/Asp racemase superfamily. The proteins of this family also share the two domain, α/β fold that is observed in KpHpxA. While these proteins have some degree of structural similarity, there is little sequence conservation amongst the members of this group (Fig. 7). Highly conserved residues include the two cysteine residues implicated in catalysis (Fig. 7, blue triangles) and several other residues that serve predominantly structural roles. These include

two isoleucine residues (Ile6 and Ile9) occupying the middle of a β -sheet (on β 1 strand) and a conserved proline residue (Pro95) that facilitates a turn from α 3 to β 4. Aside from the catalytic cysteine residues, however, none of the completely conserved residues appear in the active site of KpHpxA. It should be noted that the cysteine residue equivalent to Cys79 in KpHpxA is not conserved in PDB ID 3EIS, an arylmalonate decarboxylase, as these enzymes are reported to proceed via a different mechanism than other members of the superfamily.

KpHpxA active site and ligand binding

A comparison of unliganded and the allantoin-bound complex of KpHpxA illustrates that the enzyme does not undergo any major structural changes upon ligand binding (RMSD of α -carbons for superposition is 0.2Å). Other than a slight difference in the side chain conformation of Glu53, and the fitting of two rotamers to the density for Ser79 in the C79S/C184S KpHpxA-allantoin structure, all of the residues of the liganded structure align well with those of the unliganded structure. Alternate conformations of Ser79/Cys79 are likely important for catalysis, while the observed flexibility of the Glu53 sidechain suggests that it may act as a gate for the relatively inaccessible active site (Fig. 8). A water molecule is also within hydrogen bonding distance from Ser79 and Glu53 in the active site of the C79S/C184S KpHpxA-allantoin structure. This water molecule is not likely to directly participate in catalysis but instead may serve to help drive the movement of Glu53 upon product release.

The observed electron density in the active site for the C79S/C184S KpHpxA-allantoin structure clearly indicates that allantoin is present in its enol form (Fig. 3a). This is not a surprising result considering that allantoin is known to undergo slow racemization in solution via keto-enol tautomerization,⁶ and that the putative reaction intermediate for the racemization of allantoin is the enolate. This form of the ligand is not without precedent, and has been observed in the related structures of *Klebsiella pneumoniae* OHCU decarboxylase²⁵ and *Alcaligenes bronchisepticus* arylmalonate decarboxylase.²⁶

The two active site cysteine residues, which are substituted by serine residues in the KpHpxA double mutant, have been reported to play major roles in a two-base mechanism proposed for members of the Aspartate/Glutamate racemase superfamily.^{19,27} In the C79S/C184S KpHpxA-allantoin structure, these residues are situated on either side of the ligand (Figs. 2a and 3a). The distance between the oxygen atoms of Ser79 and Ser184 in this structure is 6.6 Å (using the rotamer of Ser79 that is closer to Ser184) and would be approximately 6.3 Å between thiols if cysteine residues were used in place of serine residues. The distances Ser79 and Ser184 to C5 of allantoin are 3.2 and 4.2 Å, respectively. It should be noted that these distances reflect the nature of the enol form of the ligand; both the (*R*)- and (*S*)- enantiomers of allantoin would be expected to bind in slightly different orientations (see modeling below).

An important structural element observed in the liganded KpHpxA structures is the presence of a putative oxyanion hole. This pocket, created by the backbone amide nitrogens of Phe80 and Gly185 (Fig. 3), which also serves to orient the hydantoin ring by interacting with the C4 oxygen atom, could stabilize negative charge that builds up at this oxygen atom along the reaction coordinate. This interaction is observed in both the allantoin (Fig. 3a) and 5-acetylhydantoin (Fig. 3b) complex structures, indicating its importance for ligand binding. In addition, the enol form of allantoin bound in the active site provides evidence that this pocket may serve to stabilize an oxyanion, because this ligand is structurally similar to the proposed enolate intermediate (see discussion of mechanism below).

One of the observed differences between the KpHpxA structure and that of hydantoin racemase is the presence of a polar region in the binding pocket of KpHpxA populated by several threonine side chains. This difference presumably stems from the dissimilarity in the substituent at the 5-position of the hydantoin ring. While hydantoin racemase accommodates non-polar, aliphatic and aromatic groups such as ethyl, isobutyl and benzyl, the ureido group at the 5-position of allantoin would require a more hydrophilic environment. This threonine-rich pocket is also likely to be an important determinant of selectivity. An examination of the two liganded structures of KpHpxA (Fig. 3) indicates that this region provides an anchoring point for the tail region of the ligand and aids in the orientation of the hydantoin ring by securing the 5-substituent in this pocket. The observation of selectivity for the (*R*)-enantiomer of 5-acetylhydantoin is likely a result of the interactions at this threonine pocket. Binding of the acetyl group of (*S*)-5-acetylhydantoin in this pocket would drive the hydantoin ring to a position almost perpendicular to that observed in the structure and would result in several unfavorable protein-ligand interactions.

Catalysis of allantoin racemization by KpHpxA

Based upon sequence similarity to members of the Aspartate/Glutamate racemase superfamily, KpHpxA enzyme is annotated as an allantoin racemase (GenBank accession no. ACG63342.1).¹² To verify this assignment of function, we tested the ability of KpHpxA to racemize the (*R*)- and (*S*)- enantiomers of allantoin. Due to slow (k_{non} of $2 \times 10^{-4} \text{ s}^{-1}$) non-enzymatic racemization of allantoin, the individual enantiomers of this compound are not commercially available. However, both isomers can be prepared enzymatically from uric acid and racemic allantoin for (*S*)- and (*R*)-allantoin, respectively (see Materials and Methods).

The difference in the CD spectra of the allantoin enantiomers provides a means to assay the racemase activity of KpHpxA. Fig. 5a shows the change in CD spectra with respect to time for the KpHpxA conversion of either (*S*)-allantoin or (*R*)-allantoin to the racemic mixture. Time courses of the above reactions are provided in Fig. 5b. KpHpxA catalyzes the racemization effectively, with a k_{cat}/K_M of $6.0 \times 10^5 \text{ M}^{-1}\text{s}^{-1}$ and a rate enhancement (k_{cat}/k_{non}) of 1.2×10^6 .

As a result of non-enzymatic decay of HIU and OHCU and slow racemization of allantoin, the efficient and economical catabolism of uric acid by a pathway such as that used by *Klebsiella sp.* requires a highly effective allantoin racemase. A high level of allantoin to allantoate throughput would necessitate a racemase with an efficiency that is equal or greater than that of the associated allantoinase enzyme. Although there is no data available for the *Klebsiella sp.* allantoinase, the catalytic efficiency of KpHpxA (k_{cat}/K_M of $6.0 \times 10^5 \text{ M}^{-1}\text{s}^{-1}$) is significantly higher than that of the metal-dependent and metal-independent allantoinase enzymes (k_{cat}/K_M of $7,000 \text{ M}^{-1}\text{s}^{-1}$ for *Phaseolus vulgaris*,²⁸ $24,000 \text{ M}^{-1}\text{s}^{-1}$ for *E. coli*⁹ and $48,000 \text{ M}^{-1}\text{s}^{-1}$ for *Pseudomonas fluorescens*¹⁰).

Members of the Aspartate/Glutamate racemase superfamily are known to employ conserved cysteines for catalysis of racemization.^{18,19} Multiple sequence alignments of several Aspartate/Glutamate racemase members with KpHpxA (Fig. 7) indicate that the catalytic residues in KpHpxA are Cys79 and Cys184. To probe the importance of these residues for KpHpxA activity, we constructed the C79S, C184S, and C79S/C184S-KpHpxA mutants and tested their ability to racemize (*R*)- or (*S*)-allantoin. Kinetic analysis by CD revealed that mutation of either of the conserved cysteine residues to serine totally inactivated the enzyme. This result is similar to the observations for hydantoin racemase from *Sinorhizobium meliloti*²⁰ and is consistent with the two-base mechanism that has been proposed for other members of this family.

Modeling of substrates in KpHpxA active site

To better understand the nature of KpHpxA active site interactions with the substrates, we performed a simple docking experiment. Both of the (*R*)- and (*S*)- isomers of allantoin were manually placed in the active site of KpHpxA and energy-minimized while keeping the positions of the protein side chains fixed. The results (Fig. 6) illustrate that the two active site cysteine residues are within a reasonable distance of allantoin C5 to participate in catalysis of the racemization reaction. In addition, the observed orientations of both isomers are consistent with our assertion that ligand binding is dominated by two main interactions, the carbonyl of C4 in the oxyanion hole, and the contacts made by the ureido tail with the threonine pocket of the KpHpxA active site.

Mechanistic implications

While there are no mechanistic studies reported on allantoin racemase, insights can be gleaned from the structural and kinetic data reported herein and results of studies on other Aspartate/Glutamate racemase superfamily members.^{18–20,27,29,30} Despite the observed asymmetry in the active site, KpHpxA catalyzes racemization of both allantoin isomers with approximately the same affinity and rate. The structures of liganded KpHpxA reveal a polar threonine pocket that interacts with the ureido tail group of allantoin and serves to orient the hydantoin ring. The other main interaction with allantoin occurs through the C4 carbonyl oxygen atom and, while mediating the lateral motion (in reference to the plane of the ring), does not preclude rotation of the molecule. These anchor points, therefore, allow for optimal positioning of either of the two isomers with respect to the two active site cysteines (Fig. 8).

Based upon the data presented herein and the known chemistry of hydantoin racemases, a mechanism for the KpHpxA-catalyzed allantoin racemase reaction is proposed (Scheme 2). Analogous to the two-base mechanism proposed for other members of this family, the two active site cysteine residues, Cys79 and Cys184, catalyze the racemization reaction by acting to both deprotonate and reprotonate allantoin at the C4 position. Deprotonation of either isomer leads to an enolate intermediate, with stabilization of the negative charge provided by the oxyanion hole. Collapse of the reactive oxyanion species drives attack of one of the thiols, leading to product formation or regeneration of the substrate. Product release is likely driven by the conformational change that the ligand undergoes after reprotonation. The change from sp^2 to sp^3 hybridization at C4 also causes a shift in the ureido tail, bringing the -NH group into an unfavorable position relative to the thiol of the deprotonating cysteine. This clash likely leads to movement of Cys79 and Glu53 away from the departing ligand, which opens the active site and allows for product release to occur.

Recent work on glutamate racemase has implicated additional residues in the active site that participate in catalysis through their interactions with the catalytic cysteine residues.^{18,27} The presence of these acidic residues was used to explain why the cysteine to serine mutants retained some level of racemase activity.^{27,31} No such acidic residues are observed within hydrogen bonding distance of either of the catalytic cysteines in the structure of KpHpxA. This is consistent with the total loss of activity observed in both of the C79S and C184S mutants.

Conclusions

In this paper, we have reported the first structural characterization of an allantoin racemase. The structures presented reveal several important features of the active site of this enzyme, including an oxyanion hole and a polar binding region that strongly interacts with the ureido tail of allantoin. In addition, measurement of the kinetic parameters by circular dichroism demonstrates that KpHpxA catalyzes the racemization of allantoin, enhancing the rate six

orders of magnitude over the non-enzymatic rate. This structural and biochemical characterization of *K. pneumoniae* allantoin racemase expands the breadth of the Aspartate/ Glutamate racemase superfamily and provides additional support for the two-base mechanism employed by this class of cofactor-independent racemases.

Materials and methods

Protein purification and crystallization

The gene encoding KpHpxA was cloned from genomic DNA from *K. pneumoniae* subsp. *pneumoniae* (Schroeter) Trevisan MGH78578 (ATCC 700721) and placed in a modified pET28 (Novagen) vector encoding an N-terminal 6-His tag by standard molecular biology techniques. The C79S, C184S and C79S/C184S mutant plasmids were made at the Cornell Protein Production and Purification Facility using site-directed mutagenesis of the native gene. Briefly, mutagenesis was performed on the *hpxA* gene by a standard PCR protocol using *Pfu*Turbo DNA polymerase (Invitrogen) and DpnI (New England Biolabs) to digest the methylated parental DNA prior to transformation. The presence of the mutated residues was verified by sequencing.

For protein expression in all cases, the plasmid was transformed into B834(DE3) (methionine auxotrophic) cells and the protein was expressed and purified as follows. For SeMet protein, the cells were grown in M9 minimal media supplemented with 0.4% glucose, MEM vitamin solution, 2 mM MgSO₄, 90 mM of FeSO₄ (25 mg/L), 100 μM CaCl₂, 40 mg/L each of 19 amino acids (methionine excluded), 50 mg/L of seleno-L-methionine and 50 mg/L kanamycin. The cells were grown at 37 °C to an O.D.₆₀₀ of 0.5 before reducing the temperature to 15 °C. After 30 min at this temperature the cells were induced with 0.5 mM isopropyl-beta-D-thiogalactopyranoside and grown for an additional 16 h. The cells were harvested by centrifugation and the pellet stored at -20 °C prior to purification. For native protein, the procedure followed was the same with the exception that lysogeny broth was used as a growth medium.

For protein purification, the pellets were thawed in buffer containing 300 mM NaCl, 10 mM imidazole, 2 mM dithiothreitol (DTT) and 50 mM sodium phosphate, pH 7.6. The cells were lysed by sonication and centrifuged to remove cellular debris. The cleared lysate was passed through a column containing pre-equilibrated Ni-NTA resin and then washed with a similar buffer containing 20 mM imidazole and 10% glycerol. The protein was eluted with buffer containing 300 mM NaCl, 2 mM DTT and 250 mM imidazole, pH 7.6 and immediately buffer exchanged into 30 mM NaCl, 2 mM DTT and 10 mM sodium acetate, pH 5.6. The protein was concentrated to 15 mg/mL using a centricon centrifugal concentrator (Amicon) and determined to be greater than 95% pure by SDS-PAGE electrophoresis. Aliquots of the protein were flash frozen immediately after buffer exchange and stored at -80 °C for crystallization trials. Crystallization was performed by the hanging-drop vapor diffusion method at 18 °C. For both the native and SeMet protein, crystals formed after 3 – 5 days in 24 – 34% PEG 400 with 0.1 M sodium acetate, pH 3.7 – 4.1. Crystals were harvested and frozen without additional cryoprotectant. For allantoin and 5-acetylhydantoin complexes, crystals were soaked for 2 h in solutions of mother liquor supplemented with 5 mM ligand.

Data collection, processing, structure determination and refinement

The SeMet data were collected at 100 K at the Northeastern Collaborative Access Team (NE-CAT) beamline 24-ID-C of the Advanced Photon Source at Argonne National Laboratory at the maximum f'' for selenium as determined by a fluorescence scan of the crystal. The SeMet dataset was collected over 360° using a 1° oscillation range. The space group was determined to be *P*6₃22 with two molecules per asymmetric unit corresponding to

a solvent content of 51%. Data were indexed and scaled using HKL2000³² and heavy atom sites were located using the SHELX suite.³³ The program autoSHARP³⁴ was used for refinement of heavy atom positions, phasing, calculation of residual maps, density modification and automated model building. The program was able to correctly place 469 of 494 residues in two chains with the correct side chains. Additional residues and water molecules were placed during iterative rounds of manual model building using Coot³⁵ followed by refinement using Refmac5.³⁶

The data for ligand bound complexes were collected at the NE-CAT beamline 24-ID-C and 24-ID-E at a wavelength of 0.979 Å. These data also indexed in space group $P6_322$ and had similar unit cell dimensions. Refinements were carried out as detailed above using the SeMet structure as a starting point. The ligands were built into difference density only after the refinement had converged. Data collection statistics are summarized in Table 1 and refinement statistics are summarized in Table 2.

Measurement of racemization activity and steady-state kinetics

KpHpxA racemization activity was calculated from changes in CD spectra over time. All reactions were carried out in buffer containing 10 mM NaCl and 10 mM HEPES, pH 7.5. Enzyme tested for activity was exchanged into the above buffer prior to analysis. (*R*)- and (*S*)-allantoin samples were prepared as follows immediately prior to measurement of rates. For (*S*)-allantoin, 20 μmoles of uric acid in 10 mM NaCl and 10 mM HEPES, pH 7.5, was incubated with 2 units of uricase from *Candida sp.* (Sigma), 5 μg of *K. pneumoniae* HIU hydrolase¹² and 5 μg of *K. pneumoniae* OHCU decarboxylase²⁵ for 30 min at 25 °C. The stereospecific production of (*S*)-allantoin was monitored by UV at 260 nm²⁵ and the final concentration was confirmed by comparison to a standard curve constructed using racemic allantoin. Upon completion of the reaction, the enzymes were removed by filtration through a 10 kDa cutoff centrifugal concentrator.

(*R*)-allantoin was produced by incubating 40 μmoles of racemic allantoin with 10 μg of *E. coli* allantoinase⁸ for 20 min at 25 °C. The progress from racemic to pure (*R*)-allantoin was monitored by CD. Upon completion of the reaction, the enzyme was removed by filtration through a 10 kDa cutoff centrifugal concentrator. Since inhibition of KpHpxA by allantoin was not observed to occur (data not shown), the resulting mixture of (*R*)-allantoin and allantoin was used without further treatment.

CD spectra and kinetics were collected on an AVIV Biomedical (Lakewood, NJ) CD spectrometer, Model 202-01. The spectra were collected at 25 °C from 190 to 260 nm with a 1 nm step size, 1 nm bandwidth and a 1 mm cell. Initial rates of reactions were calculated at various substrate concentrations and were taken from the first 10 s of the reaction (reaction less than 10% complete). The signals at 208 and 213 nm, respectively, were monitored for the (*S*)- and (*R*)- reactions. The kinetic parameters were calculated from a fit of the initial rates by the Michaelis-Menten equation using KaleidaGraph (Synergy Software).

Docking of allantoin isomers in active site, sequence alignment and structural homology search

Version 9.7.211 of the molecular modeling program, Macromodel^{37,38} was used to dock the (*R*)- and (*S*)-allantoin isomers in the active site of KpHpxA. The starting position of allantoin was derived from a superposition to the enol form of allantoin from the C79S/C184S KpHpxA-allantoin structure. The protein was truncated to a shell containing all atoms within 20 Å of the ligand. Water molecules were removed and the protein preparation utility was used to add hydrogens and to ensure proper ionic states of amino acid side chains. All of the protein atoms were frozen in place and only the allantoin ligand was

allowed to move during minimization. The calculations were completed using the AMBER* force field^{39,40} with a distance dependent dielectric that was further attenuated by a factor of 4. The energy minimization relied upon the truncated Newton conjugate gradient technique⁴¹ and was considered to have converged when the energy gradient was less than 0.01 kJ/mol.

The topology diagram was based upon the results from the PDBsum server.⁴² The sequence alignment was carried out using ClustalW⁴³ and the corresponding figure was made using the ESPript server.⁴⁴ The DALI server²¹ was used to search for structural homologues of KpHpxA. All other figures were made using PyMOL⁴⁵ and ChemBioDraw (Cambridgesoft).

Supplementary Material

Refer to Web version on PubMed Central for supplementary material.

Acknowledgments

This work was supported by NIH grant GM73220 to SEE. We thank the staff at the Northeastern Collaborative Access Team (NE-CAT) of the Advanced Photon Source, Argonne National Laboratory for advice with data collection and processing. Data collection at the NE-CAT beamlines is supported by award RR-15301 from the National Center for Research Resources at the National Institutes of Health. Use of the Advanced Photon Source is supported by the U.S. Department of Energy, Office of Basic Energy Sciences, under Contract number DE-AC02-06CH11357. We acknowledge Dr. Cynthia Kinsland of the Protein Production and Purification Facility in the Department of Chemistry and Chemical Biology for help with molecular biology and Ms. Leslie Kinsland for help with manuscript preparation. JBF would like to acknowledge the Tri-Institutional Training Program in Chemical Biology for financial support.

Abbreviations

HIU	5-hydroxyisourate
OHCU	2-oxo-4-hydroxy-4-carboxy-5-ureidoimidazoline
KpHpxA	<i>K. pneumoniae</i> allantoin racemase
CD	circular dichroism
SeMet	selenomethionyl
SAD	single-wavelength anomalous dispersion
DTT	dithiotreitol
NE-CAT	Northeastern Collaborative Access Team

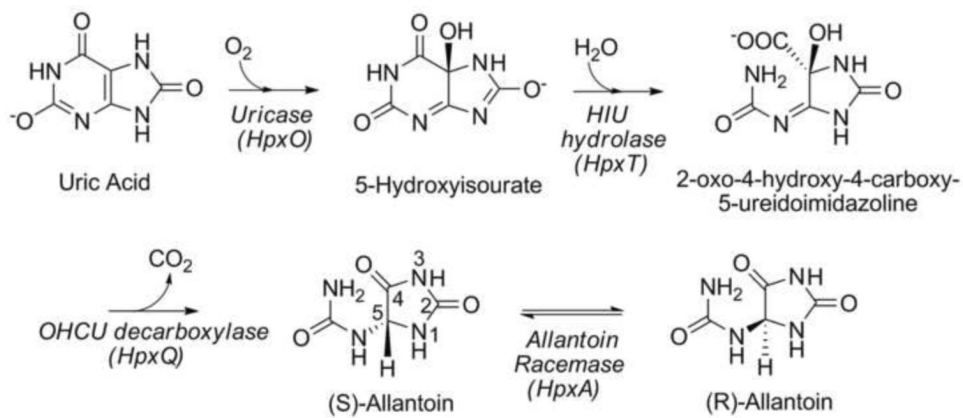
References

1. Vogels GD, Van der Drift C. Degradation of purines and pyrimidines by microorganisms. *Bacteriol. Rev.* 1976; 40:403–68. [PubMed: 786256]
2. Zrenner R, Stitt M, Sonnewald U, Boldt R. Pyrimidine and purine biosynthesis and degradation in plants. *Annu. Rev. Plant Biol.* 2006; 57:805–36. [PubMed: 16669783]
3. Kahn K, Tipton PA. Kinetic Mechanism and Cofactor Content of Soybean Root Nodule Urate Oxidase. *Biochemistry.* 1997; 36:4731–4738. [PubMed: 9125493]
4. Modric N, Derome AE, Ashcroft SJH, Poje M. Tracing and identification of uricase reaction intermediates. A direct carbon-13 NMR/isotope-labeling evidence. *Tetrahedron Lett.* 1992; 33:6691–4.

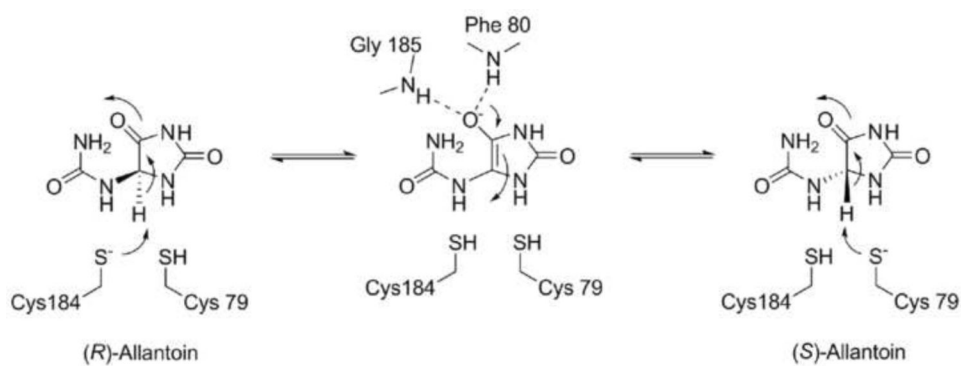
5. Ramazzina I, Folli C, Secchi A, Berni R, Percudani R. Completing the uric acid degradation pathway through phylogenetic comparison of whole genomes. *Nat. Chem. Biol.* 2006; 2:144–8. [PubMed: 16462750]
6. Kahn K, Tipton PA. Kinetics and Mechanism of Allantoin Racemization. *Bioorg. Chem.* 2000; 28:62–72.
7. Schubert KR. Products of biological nitrogen fixation in higher plants: synthesis, transport, and metabolism. *Annu. Rev. Plant Physiol.* 1986; 37:539–74.
8. Kim K, Kim MI, Chung J, Ahn JH, Rhee S. Crystal structure of metal-dependent allantoinase from *Escherichia coli*. *J. Mol. Biol.* 2009; 387:1067–74. [PubMed: 19248789]
9. Mulrooney SB, Hausinger RP. Metal ion dependence of recombinant *Escherichia coli* allantoinase. *J. Bacteriol.* 2003; 185:126–34. [PubMed: 12486048]
10. Ramazzina I, Cendron L, Folli C, Berni R, Monteverdi D, Zanotti G, Percudani R. Logical identification of an allantoinase analog (puuE) recruited from polysaccharide deacetylases. *J. Biol. Chem.* 2008; 283:23295–304. [PubMed: 18550550]
11. de la Riva L, Badia J, Aguilar J, Bender RA, Baldoma L. The hpx Genetic System for Hypoxanthine Assimilation as a Nitrogen Source in *Klebsiella pneumoniae*: Gene Organization and Transcriptional Regulation. *J. Bacteriol.* 2008; 190:7892–7903. [PubMed: 18849434]
12. Pope SD, Chen L-L, Stewart V. Purine Utilization by *Klebsiella oxytoca* M5al: Genes for Ring-Oxidizing and -Opening Enzymes. *J. Bacteriol.* 2009; 191:1006–1017. [PubMed: 19060149]
13. Okumura I, Kondo K, Miyake Y, Itaya K, Yamamoto T. Stereospecificity of conversion of uric acid into allantoinic acid by enzymes of *Canadida utilis*. *J. Biochem.* 1976; 79:1013–9. [PubMed: 986391]
14. Okumura I, Yamamoto T. Enzymic racemization of allantoin. *J. Biochem.* 1978; 84:891–5. [PubMed: 568622]
15. Van der Drift L, Vogels GD, Van der Drift C. Allantoin racemase: a new enzyme from *Pseudomonas* species. *Biochim. Biophys. Acta.* 1975; 391:240–8. [PubMed: 237557]
16. Nam SH, Park HS, Kim HS. Evolutionary relationship and application of a superfamily of cyclic amidohydrolase enzymes. *Chem. Rec.* 2005; 5:298–307. [PubMed: 16211624]
17. Altenbuchner J, Siemann-Herzberg M, Syltatk C. Hydantoinases and related enzymes as biocatalysts for the synthesis of unnatural chiral amino acids. *Curr. Opin. Biotechnol.* 2001; 12:559–63. [PubMed: 11849938]
18. Hwang KY, Cho CS, Kim SS, Sung HC, Yu YG, Cho Y. Structure and mechanism of glutamate racemase from *Aquifex pyrophilus*. *Nat. Struct. Biol.* 1999; 6:422–6. [PubMed: 10331867]
19. Martinez-Rodriguez S, Andujar-Sanchez M, Neira JL, Clemente-Jimenez JM, Jara-Perez V, Rodriguez-Vico F, Las Heras-Vazquez FJ. Site-directed mutagenesis indicates an important role of cysteines 76 and 181 in the catalysis of hydantoin racemase from *Sinorhizobium meliloti*. *Protein Sci.* 2006; 15:2729–38. [PubMed: 17132860]
20. Andujar-Sanchez M, Martinez-Rodriguez S, Heras-Vazquez FJ, Clemente-Jimenez JM, Rodriguez-Vico F, Jara-Perez V. Binding studies of hydantoin racemase from *Sinorhizobium meliloti* by calorimetric and fluorescence analysis. *Biochim. Biophys. Acta.* 2006; 1764:292–8. [PubMed: 16406752]
21. Holm L, Kaarianinen S, Rosenstrom P, Schenkel A. Searching protein structure databases with DaliLite v.3. *Bioinformatics.* 2008; 24:2780–2781. [PubMed: 18818215]
22. Watabe K, Ishikawa T, Mukohara Y, Nakamura H. Purification and characterization of the hydantoin racemase of *Pseudomonas* sp. strain NS671 expressed in *Escherichia coli*. *J. Bacteriol.* 1992; 174:7989–95. [PubMed: 1459947]
23. Martinez-Rodriguez S, Las Heras-Vazquez FJ, Clemente-Jimenez JM, Rodriguez-Vico F. Biochemical characterization of a novel hydantoin racemase from *Agrobacterium tumefaciens* C58. *Biochimie.* 2004; 86:77–81. [PubMed: 15016445]
24. Suzuki S, Onishi N, Yokozeki K. Purification and characterization of hydantoin racemase from *Microbacterium liquefaciens* AJ 3912. *Biosci. Biotechnol. Biochem.* 2005; 69:530–6. [PubMed: 15784981]

25. French JB, Ealick SE. Structural and mechanistic studies on *Klebsiella pneumoniae* 2-Oxo-4-hydroxy-4-carboxy-5-ureidoimidazoline decarboxylase. *J. Biol. Chem.* 2010; 285:35446–35454. [PubMed: 20826786]
26. Obata R, Nakasako M. Structural basis for inverting the enantioselectivity of arylmalonate decarboxylase revealed by the structural analysis of the Gly74Cys/Cys188Ser mutant in the liganded form. *Biochemistry.* 2010; 49:1963–9. [PubMed: 20136121]
27. Glavas S, Tanner ME. Active site residues of glutamate racemase. *Biochemistry.* 2001; 40:6199–204. [PubMed: 11371180]
28. Raso MJ, Pineda M, Piedras P. Tissue abundance and characterization of two purified proteins with allantoinase activity from French bean (*Phaseolus vulgaris*). *Physiol. Plant.* 2007; 131:355–66. [PubMed: 18251875]
29. Las Heras-Vazquez FJ, Martinez-Rodriguez S, Mingorance-Cazorla L, Clemente-Jimenez JM, Rodriguez-Vico F. Overexpression and characterization of hydantoin racemase from *Agrobacterium tumefaciens* C58. *Biochem. Biophys. Res. Commun.* 2003; 303:541–7. [PubMed: 12659852]
30. Ohtaki A, Nakano Y, Iizuka R, Arakawa T, Yamada K, Odaka M, Yohda M. Structure of aspartate racemase complexed with a dual substrate analogue, citric acid, and implications for the reaction mechanism. *Proteins.* 2008; 70:1167–74. [PubMed: 17847084]
31. Glavas S, Tanner ME. Catalytic acid/base residues of glutamate racemase. *Biochemistry.* 1999; 38:4106–13. [PubMed: 10194325]
32. Otwinowski, Z.; Minor, W.; Carter, Charles W., Jr. *Methods in Enzymology.* Vol. Volume 276. Academic Press; 1997. Processing of X-ray diffraction data collected in oscillation mode; p. 307-326.
33. Sheldrick GM. A short history of SHELX. *Acta Crystallogr. A.* 2008; 64:112–122. [PubMed: 18156677]
34. Vonrhein C, Blanc E, Roversi P, Bricogne G. Automated structure solution with autoSHARP. *Methods Mol. Biol.* 2007; 364:215–30. [PubMed: 17172768]
35. Emsley P, Cowtan K. Coot: model-building tools for molecular graphics. *Acta Crystallogr. D.* 2004; 60:2126–32. [PubMed: 15572765]
36. Murshudov GN, Vagin AA, Dodson EJ. Refinement of macromolecular structures by the maximum-likelihood method. *Acta Crystallogr. D Biol. Crystallogr.* 1997; 53:240–55. [PubMed: 15299926]
37. Mohamadi F, Richards NGJ, Guida WC, Liskamp R, Lipton M, Caulfield C, Chang G, Hendrickson T, Still WC. MacroModel - an Integrated Software System for Modeling Organic and Bioorganic Molecules Using Molecular Mechanics. *J. Comput. Chem.* 1990; 11:440–67.
38. Still, WC.; Mohamadi, F.; Richards, NGJ.; Guida, WC.; Liskamp, R.; Lipton, M.; Caulfield, C.; Chang, G.; Hendrickson, T. *MacroModel 2.0* edit. Columbia University; New York, NY: 1999.
39. Weiner SJ, Kollman PA, Case DA, Singh UC, Ghio C, Alagona G, Profeta S Jr, Weiner P. A new force field for molecular mechanical simulation of nucleic acids and proteins. *J. Am. Chem. Soc.* 1984; 106:765–84.
40. Weiner SJ, Kollman PA, Nguyen DT, Case DA. An all atom force field for simulations of proteins and nucleic acids. *J. Comput. Chem.* 1986; 7:230–52.
41. Ponder JW, Richards FM. An efficient Newton-like method for molecular mechanics energy minimization of large molecules. *J. Comput. Chem.* 1987; 8:1016–24.
42. Laskowski RA. PDBsum new things. *Nucleic Acids Res.* 2009; 37:D355–9. [PubMed: 18996896]
43. Larkin MA, Blackshields G, Brown NP, Chenna R, McGettigan PA, McWilliam H, Valentin F, Wallace IM, Wilm A, Lopez R, Thompson JD, Gibson TJ, Higgins DG. Clustal W and Clustal X version 2.0. *Bioinformatics.* 2007; 23:2947–8. [PubMed: 17846036]
44. Gouet P, Courcelle E, Stuart DI, Metz F. ESPript: analysis of multiple sequence alignments in PostScript. *Bioinformatics.* 1999; 15:305–8. [PubMed: 10320398]
45. DeLano, WL. *The PyMOL Molecular Graphics System.* DeLano Scientific; San Carlos, CA: 2002.
46. May M, Mehboob S, Mulhearn DC, Wang Z, Yu H, Thatcher GR, Santarsiero BD, Johnson ME, Mesecar AD. Structural and functional analysis of two glutamate racemase isozymes from

Bacillus anthracis and implications for inhibitor design. *J. Mol. Biol.* 2007; 371:1219–37.
[PubMed: 17610893]



Scheme 1.
Purine catabolic pathway in *K. pneumoniae*.^{11,12}

**Scheme 2.**

Proposed mechanism of catalysis for racemization of allantoin by KpHpxA.

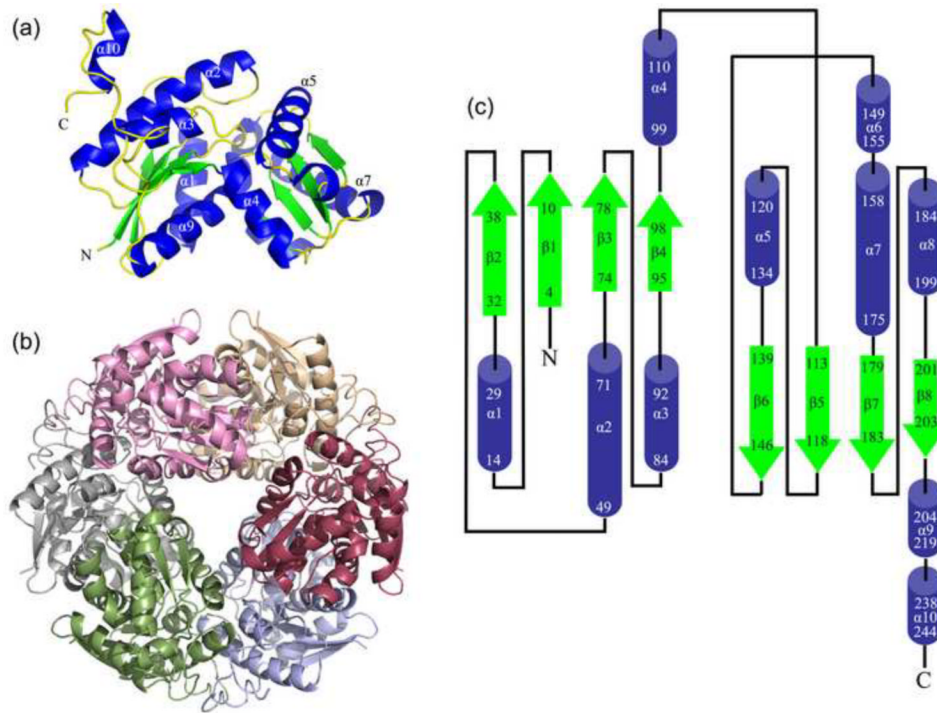


Fig. 1. Structure of KpHpxA. (a) KpHpxA protomer. (b) Hexameric structure of KpHpxA seen in the crystals and confirmed by size exclusion chromatography. (c) Topology diagram of KpHpxA. Helices are shown as blue cylinders and strands as green arrows. The numbers correspond to the residue numbers of the first and last amino acid of each secondary structure element. The N and C termini are marked with an N and C, respectively.

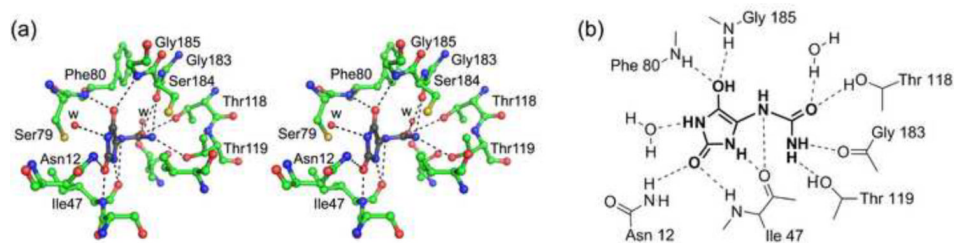


Fig. 2. Active site of KpHpxA. (a) Stereodigram of the active site of KpHpxA in complex with allantoin. The structure shown (carbon atoms in green, nitrogen atoms in blue, and oxygen atoms in red) is that of the C79S/C184S double mutant with allantoin bound (C in black, N in blue, O in red). Waters are represented as red spheres and are labeled with 'w'. Putative hydrogen bonds are illustrated with dashed lines. (b) Schematic drawing of the active site contacts between KpHpxA and allantoin. Dashed lines indicate putative hydrogen bonds. Cys79 and Cys184 are not shown.

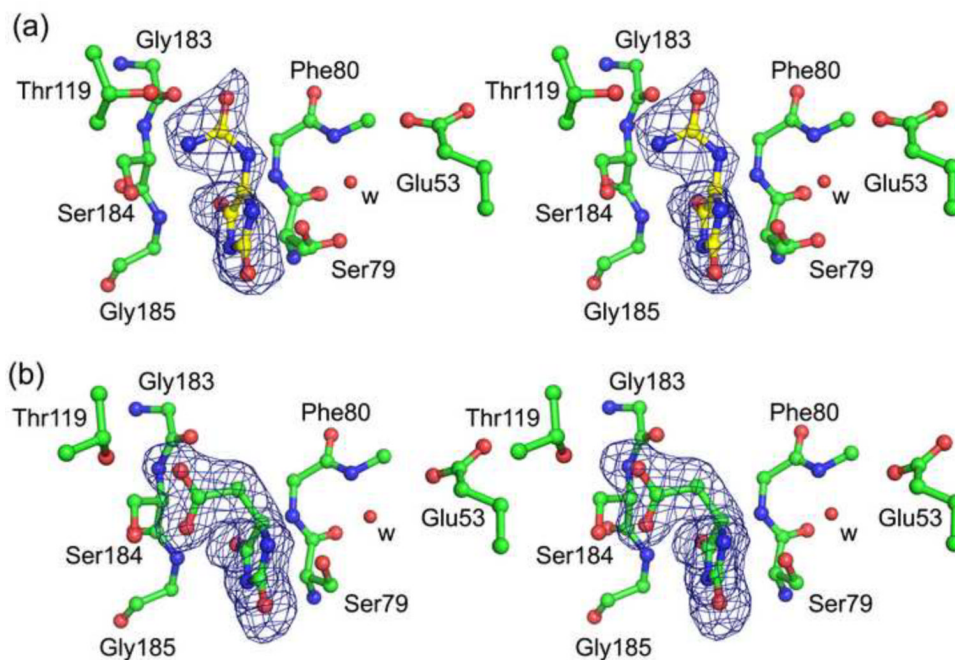


Fig. 3. Ligands bound to KpHpxA. (a) Stereodiagram of allantoin bound to the C79S/C184S KpHpxA double mutant. (b) Stereodiagram of 5-acetylhydantoin bound to the C79S/C184S KpHpxA double mutant. In both cases carbon atoms are green, oxygen atoms are red and nitrogen atoms are blue. The red sphere labeled with 'w' is a water molecule. The sidechain of Phe80 has been omitted for clarity. The electron density in both cases is from difference maps generated before the addition of the ligand molecule into the model and are contoured at 3σ .

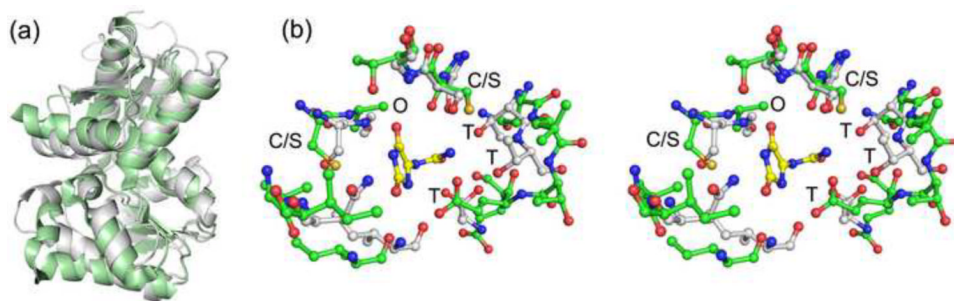


Fig. 4. Superposition of KpHpxA and the hydantoin racemase from *P. horikoshii* (2EQ5). (a) Secondary structural superposition of the protomers from KpHpxA (white) and 2EQ5 (green). (b) Stereodiagram of the superposition of the active sites of KpHpxA (white carbon atoms, blue nitrogen atoms, and red oxygen atoms) and 2EQ5 (green carbon atoms) with allantoin shown (yellow carbon atoms). The two active site cysteines (serines in KpHpxA-allantoin structure) are labeled with C/S, the putative oxyanion hole is designated with an O, and each of the threonine residues that interact with the 'tail' region of allantoin in KpHpxA is labeled with T.

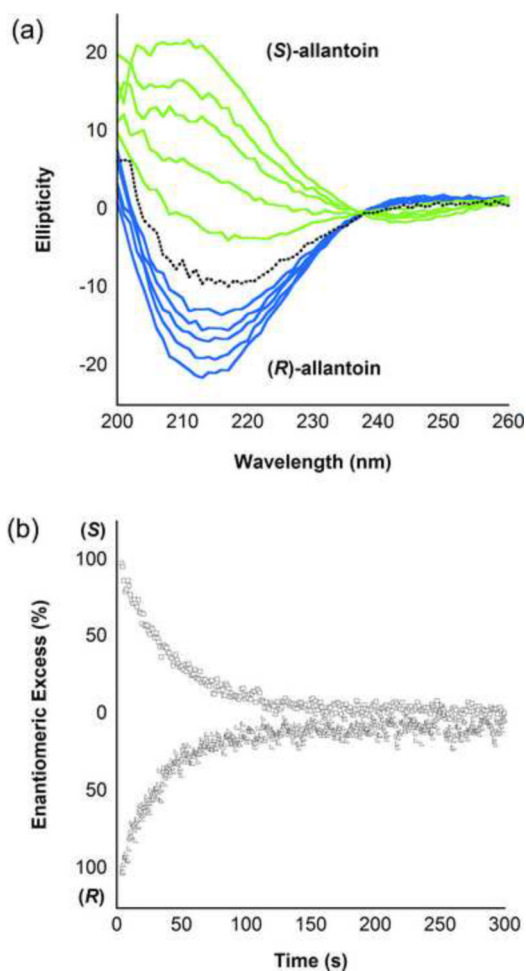


Fig. 5. Allantoin racemization catalyzed by KpHpxA. (a) CD Spectra of the racemization of (*S*)-allantoin (green curves) and (*R*)-allantoin (blue curves) to the racemic mixture (black dotted line) over time. In both cases, the starting concentration of allantoin was 2 mM and the curves represent 20 second time intervals from 0 to 80 seconds. (b) Time course of KpHpxA catalyzed racemization of (*S*)-allantoin (open squares, monitored at 208 nm) and (*R*)-allantoin (open triangles, monitored at 213 nm) to the racemic mixture.

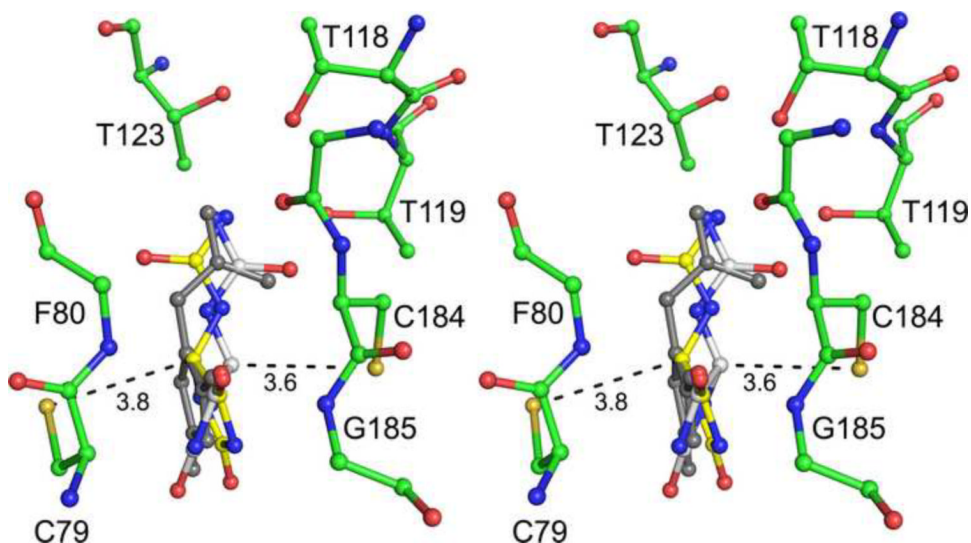


Fig. 6. Allantoine isomers in KpHpxA active site. Stereodiagram of the (*R*)- (white carbon atoms) and the (*S*)- (yellow carbon atoms) isomers of allantoine docked in the active site of KpHpxA. The observed distances between the two active site cysteines and C5 of the respective modeled allantoine isomers are shown in Ångstroms. The observed enol form of allantoine is shown in grey.

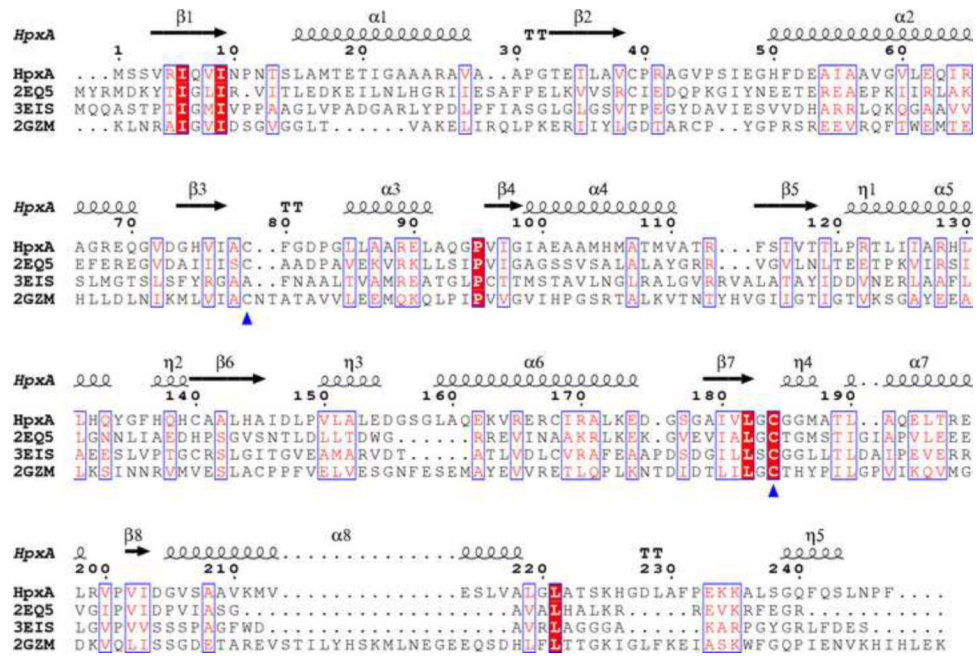


Fig. 7. Sequence alignment of several Aspartate/Glutamate racemase superfamily members. The sequences were aligned using ClustalW⁴³ and the figure was produced using the ESPrnt server.⁴⁴ The four sequences are the *K. pneumoniae* allantoic racemase (HpxA), *P. horikoshii* hydantoin racemase (2EQ5), *Bordetella bronchiseptica* Arylmalonate decarboxylase (3EIS²⁶), and *Bacillus anthracis* glutamate racemase (2GZM⁴⁶). Red boxes with white lettering are completely conserved residues while boxes with red letters on a white background are regions of sequence similarity. The blue triangles indicate the two conserved cysteines, and the numbering and secondary structural elements shown correspond to the KpHpxA structure presented herein.

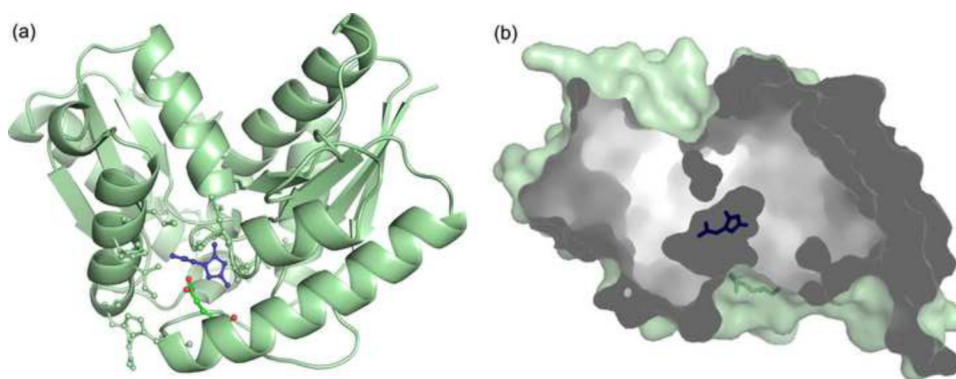


Fig. 8. Access to the KpHpxA active site. (a) The structure of KpHpxA is shown (pale green, ribbon and ball-and-stick) with allantoic acid bound (blue, ball-and-stick). Glu53, which may serve as a gate for the active site, is shown in ball-and-stick with green carbon atoms and red oxygen atoms. (b) Cutaway surface representation of KpHpxA shown with allantoic acid bound (blue stick representation). The putative gating residue, Glu53, is shown in green stick representation. Fig. 8b is rotated 90° about the y-axis relative to Fig. 8a.

Table 1

Data Collection Statistics.

	KpHpxA - SeMet	KpHpxA - C79S/C184S - allantoin	KpHpxA - C79S/C184S - 5-acetylhydantoin
resolution (Å)	50.0 - 2.1	50.0 - 2.0	50.0 - 1.82
wavelength (Å)	0.9792	0.9791	0.9791
beamline	24-ID-C	24-ID-E	24-ID-E
space group	<i>P</i> 6 ₃ 22	<i>P</i> 6 ₃ 22	<i>P</i> 6 ₃ 22
a (Å)	124.8	124.9	125.0
c (Å)	126.8	127.0	127.0
no. of reflections	106 706	197 739	805 670
unique reflections	28 561	39 452	52 509
Average I/σ	15.0 (2.1)	25.4 (4.3)	47.0 (7.9)
redundancy	3.7 (3.5)	5.0 (4.5)	15.3 (11.3)
completeness (%)	94.6 (99.6)	98.3 (98.2)	99.9 (100.0)
R_{sym}^a (%)	9.7 (40.1)	9.6 (38.1)	7.0 (30.1)

Numbers in parentheses correspond to the highest resolution shell

^a $R_{sym} = \frac{\sum \sum |I_i - \langle I \rangle|}{\sum \langle I \rangle}$, where $\langle I \rangle$ is the mean intensity of the N reflections with intensities I_i and common indices h, k, l .

Table 2

Data Refinement Statistics.

	KpHpxA - SeMet	KpHpxA - C79S/C184S - allantoin	KpHpxA - C79S/C184S - 5-acetylhydantion
resolution (Å)	50.0 - 2.1	50.0 - 2.0	50.0 - 1.82
no. of protein atoms	3542	3573	3518
no. of ligand atoms	0	14	22
no. of water atoms	190	302	446
no. of reflections in working set	32 766	37 463	49 799
no. of reflections in test set	1 740 (5 %)	1 974 (5 %)	2675 (5%)
<i>R</i> factor ^a (%)	20.5	22.2	20.8
<i>R</i> _{free} ^b (%)	23.9	24.6	22.2
rmsd bonds (Å)	0.007	0.005	0.005
rmsd angles (°)	1.013	0.927	0.927
mean <i>B</i> factor (Å ²)	32.9	31.6	19.9
Ramachandran plot			
most favored (%)	94.3	95.2	95.2
additionally allowed (%)	5.7	4.8	4.8
generously allowed (%)	0.0	0.0	0.0
disallowed (%)	0.0	0.0	0.0

^a *R* factor = $\frac{\sum |hkl| |F_{obs}| - k |F_{calc}|}{\sum |hkl| |F_{obs}|}$, where *F*_{obs} and *F*_{calc} are observed and calculated structure factors respectively.

^b For *R*_{free}, the sum is extended over a subset of reflections (5%) excluded from all stages of refinement.